Optimizing Antibacterial Activity and Wettability of 304 Stainless-steel Through Laser Pulse Overlap Control

Hedieh Pazokian[a], Sahar Sohrabi[b,*]

[a]Photonics and Quantum Technologies Research School, Nuclear Science and Technology Research Institute, Iran
[b]Department of Physics, Iran University of Science & Technology, Iran

Corresponding author email: s.sohrabiiust@gmail.com

Received: May 30, 2026, Revised: Oct. 04, 2026, Accepted: Oct. 25, 2026, Available Online: Nov. 08, 2026
DOI: Will be added soon.

ABSTRACT— This study investigates the influence of overlapping Nd:YAG laser pulses on the surface properties of 304 stainless-steel and the subsequent effect on its antibacterial performance. The degree of pulse overlap was controlled by varying the beam scanning velocity. The irradiated surfaces were characterized using Field Emission Scanning Electron Microscopy (FESEM) for morphology, Energy-dispersive X-ray spectroscopy (EDS) for chemical composition, and the sessile drop method for water contact angle measurement. The antibacterial efficacy of the treated surfaces was evaluated by assessing Escherichia coli (E. coli) bacterial adhesion. Results indicate that laser pulse overlap is a critical parameter, directly impacting processing efficiency and the resultant surface modification. The sample treated with 81% pulse overlap (achieved at a scanning velocity of 400 µm/s, a fluence of 5 J/cm², a pulse repetition rate of 10 Hz, and a spot diameter of 220 µm) exhibited the highest bactericidal activity, reducing bacterial adhesion by 62%.

KEYWORDS: Antibacterial surfaces, Bactericidal activity, Laser pulse overlapping, Nanostructures, Stainless-steel

I. INTRODUCTION

The growing prevalence of antibiotic-resistant bacteria and associated public health challenges have intensified the need for developing antibacterial surfaces, attracting significant scientific attention [1], [2]. The fundamental strategy for creating such surfaces is to prevent the initial bacterial attachment. This adhesion is a complex process governed by interactions such as van der Waals forces and the electrical double layer [3]. While several factors, including surface charge [4], surface tension [5] and also bacterial properties like size [6], influence the rate of bacterial adhesion, studies indicate that surface wettability and topography are among the most critical parameters [7], [8]. For instance, both superhydrophobic [9], [10] and superhydrophilic-nanostructured [11] surfaces have demonstrated antibacterial properties. These wettability states are, in turn, determined by two key factors: the surface's chemical composition and its morphological features. Due to their unique properties, materials with superhydrophilic or superhydrophobic characteristics have wide-ranging applications in biological and biomedical fields [12].

Laser irradiation has emerged as a clean and versatile method for surface modification. During laser-material interaction, different mechanisms such as melting, vaporization, plasma formation and phase explosion can occur [13]. The dominant mechanism and the efficiency of the interaction are determined by surface properties (e.g., absorption coefficient) and laser parameters, including fluence and pulse overlap. These factors ultimately control the formation of micro/nanostructures and chemical changes on the surface. Since wettability is a function of both surface morphology and chemical composition [14], optimizing laser parameters allows for the

[Downloaded from mail.ijop.ir on 2026-11-23]

precise tailoring of surface wettability to control bacterial adhesion.

While many researchers have utilized femtosecond lasers to fabricate antibacterial surfaces, such as texturing titanium [15] or nanostructuring surfaces to inhibit biofilm growth [16], nanosecond lasers offer greater potential for industrial-scale applications. For example, R.K. Gupta *et al*. (2019) analyzed how Nd:YAG laser irradiation modifies the wettability and chemistry of 304 stainless-steel to enhance its antibacterial and corrosion resistance [17]. A subsequent study in 2025 [18] presented the effects of nanosecond laser texturing on the topography, chemistry, and bactericidal activity of titanium. However, a critical parameter often overlooked in such experiments is the effect of laser pulse overlap, which is the focus of the present study.

During irradiation of samples with a scanning beam, N pulses is required for the laser beam with the constant velocity of v, to move an area equal to laser beam spot diameter ($2r$). The number of pulses, N, can be calculated using [19]:

$$N = \frac{2r}{b}. \quad (1)$$

The distance travelled by the laser beam between two consequent pulses, b, can be calculated by [19]:

$$b = \frac{v}{f}, \quad (2)$$

where f is the pulse repetition rate.

The laser pulse overlapping (S_{pulse}) can be calculated by [20]:

$$S_{pulse}(\%) = \left[1 - \left(\frac{v}{2rf}\right)\right] \times 100, \quad (3)$$

As it can be seen from the Eq. (3), the pulse overlapping area depends on the laser beam scanning velocity, the pulse repetition rate and the laser beam spot size.

Building on our previous work [21], which investigated the influence of laser fluence on the bacterial adhesion rate of stainless-steel, this study addresses a critical scaling parameter: laser pulse overlap. The prior results demonstrated that irradiation at fluences above the ablation threshold reduced bacterial attachment compared to the pristine surface. However, to treat larger, practically relevant areas, the laser beam must be scanned across the surface. Consequently, the scanning velocity- and the resulting degree of laser pulse overlap- becomes a critical parameter governing the modified surface properties.

This paper investigates the effect of laser pulse overlap on the antibacterial activity of 304 stainless-steel, with particular attention to its significant impact on the economic feasibility of the method. Given the importance of cost-effectiveness in practical solutions [22]-[25], machine learning has been employed in related studies to model parameters such as price, surface energy, and roughness [26]-[28]. In the present work, samples were irradiated with a pulsed Nd:YAG laser at a fluence of 5 J/cm² and a repetition rate of 10 Hz, with the pulse overlap varied through different scanning velocities. The modified surfaces were characterized for chemical and morphological changes, wetting properties, and bacterial adhesion.

II. MATERIALS AND METHODS

A. *Sample Preparation*

Commercial stainless-steel sheets (1 mm thickness) were sectioned into 1×1 cm² coupons. Prior to laser irradiation, the substrates underwent sequential ultrasonic cleaning in deionized (DI) water and 98% ethanol for 15 minutes each to eliminate surface contaminants and residual organic impurities.

B. *Laser Surface Treatment*

Laser micro/nanostructuring was performed using a pulsed Q-switched Nd:YAG laser operating at a fundamental wavelength of λ=1064 nm with a pulse duration of τ=16 ns and a repetition rate of f=10 Hz. The laser fluence was maintained at 5 J/cm², exceeding the stainless-steel ablation threshold (~3 J/cm²). The focused beam exhibited a Gaussian

[Downloaded from mail.ijop.ir on 2026-11-23]

profile with a nominal spot diameter of $2\omega_0 \approx 220$ μm.

The specimens were mounted on a precision motorized X–Y translation stage. To systematically evaluate the influence of spatial pulse overlap, the scanning velocity (V) along the X-direction was varied at 60, 200, 300, and 400 μm/s. The inter-track line spacing in the Y-direction was fixed at 250 μm, thereby preventing cross-track overlap and ensuring that the observed structural variations were governed solely by the linear pulse overlap along the scan path.

C. *Surface Characterization*

When you cannot upload your manuscript file, due to its higher volume than the site limit, you can reduce the size by:

- Wettability Analysis: The wettability of pristine and irradiated samples was evaluated using the sessile drop method. A 4 μL deionized water droplet was placed on the surface at room temperature, and its image was captured using an optical microscope. The static water contact angle (WCA) was measured by analyzing the image with ImageJ software. The reported WCA for each sample is the average of three measurements, with an error margin of ±2°.
- Morphology and Chemical Composition: The surface topography and laser-induced hierarchical micro/nanostructures were characterized using Field Emission Scanning Electron Microscopy (FE-SEM, MIRA3 TESCAN). The corresponding changes in surface elemental composition were quantitatively analyzed via Energy-Dispersive X-ray Spectroscopy (EDS, ARYA Electron Optic) at an accelerating voltage of 15 kV.

D. *Bacterial Adhesion Test*

The antibacterial properties were assessed via a bacterial adhesion test using Escherichia coli (E. coli). The bacteria were cultured on Mueller-Hinton agar plates at 37°C. The specific inoculum preparation and testing protocol followed the method detailed in our previous work [21].

The samples were washed 3 times with PBS buffer to remove non-adhered bacteria. Then, 10 μL suspension was taken from each well and diluted with 90 μL of phosphate buffer (1:10). Then, the samples were placed on the slide and prepared slowly with the heat of the smear flame. After that, gram staining method was used. The number of adhered bacteria on the samples were calculated. The relative eradication of the bacteria (E) can be calculated by [29]:

$$E(\%) = \left[1 - \left(\frac{D}{F}\right)\right] \times 100, \quad (4)$$

where D and F are the number of adhered bacteria on the irradiated and control sample, respectively.

III. Results and Discussion

A. *Surface Morphological Analysis*

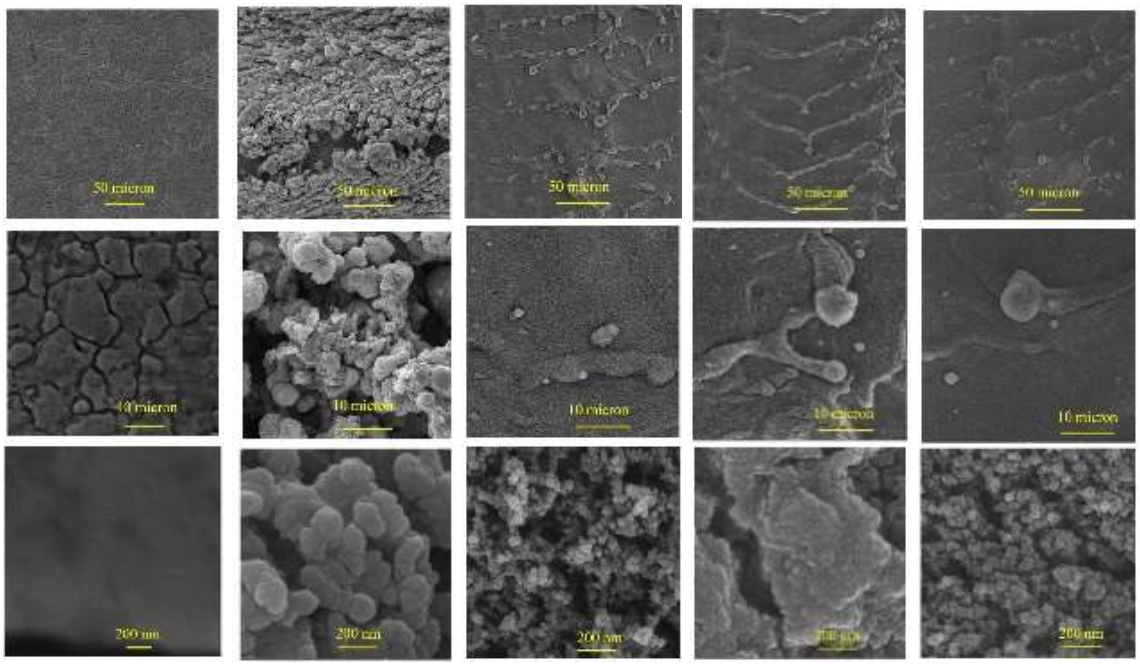
Figure 1 shows Scanning Electron Microscopy (FESEM) images of (a) the pristine stainless-steel and samples irradiated at a fluence of 5 J/cm² and a repetition rate of 10 Hz, with scanning velocities of (b) 60, (c) 200, (d) 300, and (e) 400 μm/s.

The pristine stainless-steel surface predominantly exhibits initial grinding tracks and localized micro-cracks (Fig. 1(a)). Upon laser irradiation, the surface topography undergoes pronounced restructuring, yielding distinct multi-scale micro- and nanoscale morphologies across all treated substrates.

The spatial pulse overlap—controlled via the scanning velocity—governs the surface morphology. At the lowest velocity of 60 μm/s (highest pulse overlap of ≈97.3%), high cumulative thermal accumulation induces severe surface melting, yielding a dense, quasi-continuous layer of micro-corrugations and resolidified ridges (Fig. 1(b)). Conversely, increasing the scanning velocity to 200, 300, and 400 μm/s (reducing the overlap to 90.9%, 86.4%, and 81.8%, respectively) suppresses melt-pool coalescence. Consequently, the

[Downloaded from mail.ijop.ir on 2026-11-23]

individual irradiation tracks become distinguishable, characterized by discrete, sporadic micro-bumps rather than a continuous melt layer (Fig. 1(c)–1(e)).



(a) (b) (c) (d) (e)

Fig. 1. FESEM images of the (a) pristine stainless-steel and samples irradiated at the fluence of 5 J/cm^2, the pulse repetition rate of 10 Hz and the scanning velocity of (b) 60, (c) 200, (d) 300 and (e) 400. Nanostructures are observed on the surface of all irradiated samples, while microstructures are also seen on the surface of the sample irradiated with scanning velocity of 60.

High-magnification SEM inspection reveals that all irradiated tracks are covered with dense, self-organized nanostructures. Notably, the characteristic feature size of these nanostructures decreases monotonically with increasing scanning speed. This refinement is directly correlated with the reduced cumulative heat accumulation per unit area at higher translation speeds, which minimizes melt relaxation and promotes rapid non-equilibrium quenching, yielding finer nanoscale features.

B. *Chemical Changes*

Ambient laser processing induces simultaneous physical ablation and localized thermochemical reactions. The interaction of the high-temperature laser-induced plasma plume with ambient air primarily triggers two competing mechanisms: extensive surface oxidation (formation of polar oxygenated species) and localized carbonization.

Quantitative EDS analysis (Table 1) demonstrates that laser irradiation markedly alters the surface elemental stoichiometry. A substantial increase in atomic oxygen content is detected across all processed samples relative to the pristine substrate, reaching its maximum at the lowest scanning velocity (60 μm/s) due to prolonged thermal exposure. Concurrently, the sample processed at 60 μm/s displays a noticeable rise in carbon concentration. In contrast, higher scanning speeds (200–400 μm/s) show a progressive attenuation of carbon content alongside sustained surface oxidation. While minor fluctuations in the primary metallic constituents (Fe, Cr, Ni) were detected, the functional behavior governing wettability and anti-biofouling performance is primarily mediated by the oxygen-to-carbon (O/C) ratio and surface oxidation states.

As shown in Table 1, while the carbon content remains largely unchanged from the pristine

[Downloaded from mail.ijop.ir on 2026-11-23]

sample, the oxygen content increases by approximately 13-fold in all irradiated samples.

Table 1. Atom (%) of components in the non-irradiated stainless-steel and the samples irradiated at the fluence of 5 J/cm^2, the repetition rate of 10 Hz and the scanning velocities of 60, 200, 300 and 400 μm/s.

Atom (%) *v* (μm/s)	O	C	Cr	Fe	Ni
Non-irradiated	2.12	20.90	15.98	56.44	4.65
60	32.06	24.66	8.95	31.90	3.24
200	26.00	18.42	13.70	39.25	2.63
300	28.66	19.27	12.75	37.04	2.28
400	27.53	14.77	14.13	40.90	2.67

C. *Surface Wettability*

As established, surface wettability significantly influences the material's performance in biological applications. Therefore, the wettability of the samples was characterized before and after laser irradiation using the sessile drop method. The measured WCAs for the pristine and irradiated samples are presented in Table 2.

The wettability of the samples, characterized by WCA measurements, revealed three distinct regimes (Table 2). The pristine sample was hydrophilic, while laser irradiation induced significant changes: the sample treated at the lowest scanning velocity (60 μm/s) became hydrophobic, and those irradiated at higher velocities (200, 300, and 400 μm/s) became superhydrophilic.

Table 2. Wettability of the non-irradiated stainless-steel surface and the surfaces irradiated at the fluence of 5 J/cm^2, the repetition rate of 10 Hz and the scanning velocities of 60, 200, 300 and 400.

v (μm/s)	Wettability
0	Hydrophilic (50°)
60	Hydrophobic (120°)
200	Superhydrophilic (0°)
300	Superhydrophilic (0°)
400	Superhydrophilic (0°)

These wettability transitions can be explained by the interplay between the chemical and morphological modifications detailed in previous sections. Chemically, the sample irradiated at 60 μm/s exhibited a significant increase in carbon content (Table 1), which promotes hydrophobicity. In contrast, the samples treated at higher velocities showed a marked increase in oxygen content- forming polar functional groups- and a concurrent decrease in carbon content, which favors hydrophilicity.

Morphology also plays a critical role. The hierarchical micro/nanostructures formed at 60 μm/s (Fig. 1b) facilitate a Cassie-Baxter state, where air is trapped beneath the water droplet, resulting in a high contact angle despite the presence of some oxygen. Conversely, the uniform nanostructures with smaller feature sizes (approximately 40 nm) found on samples irradiated at higher velocities promote complete wetting via a Wenzel state, where the liquid penetrates the surface textures. The combination of this nanoscale morphology and the high surface oxygen content synergistically leads to the observed superhydrophilicity.

D. *Bacterial adhesion rate test*

Figure 2 shows the relative bacterial eradication for the irradiated samples, calculated using Eq. (4). The results indicate that bacterial eradication increases with scanning velocity under the given irradiation conditions. The sample scanned at 400 μm/s exhibited the highest bactericidal activity, with approximately 62% relative eradication.

The observed enhancement in antibacterial properties aligns with existing literature on superhydrophilic surfaces [30]-[32]. While all laser-irradiated, nanostructured samples demonstrated a lower bacterial adhesion rate than the pristine surface, the scanning velocity—and consequently, the degree of laser pulse overlap—proved to be a critical factor determining the level of bactericidal efficacy. This dependence can be explained by the laser-induced chemical and morphological changes detailed in previous sections.

Furthermore, surface nanostructures can inhibit bacterial adhesion by reducing the effective contact area and exerting mechanical stress on the cell wall [33]. Specifically, nanostructures

[Downloaded from mail.ijop.ir on 2026-11-23]

with sharp features can physically puncture or strain the bacterial cell membrane, compromising its integrity and leading to the leakage of cellular components and cell death [34]. A comparison of Fig. 1 and Fig. 2 reveals that samples with smaller, sharper nanostructures exhibited higher bactericidal activity. This supports the mechanism that such nanostructures inflict greater mechanical damage on bacterial membranes.

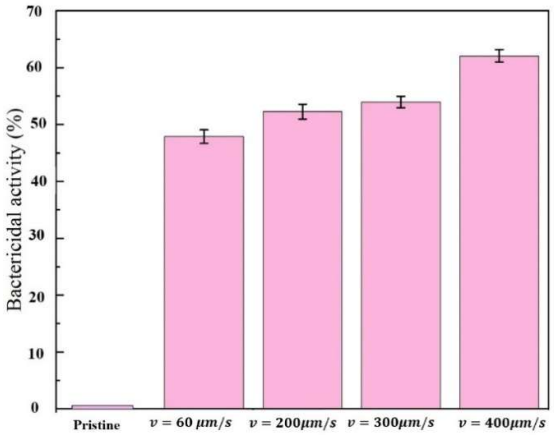


Fig. 2. Bactericidal efficacy vs. E. coli for samples laser-treated at 5 J/cm². The plot shows the relative bacterial eradication as a function of scanning velocity. A clear trend of increasing antibacterial activity with scanning velocity is observed, with the pristine sample exhibiting zero efficacy.

As the results demonstrate, varying the scanning velocity while keeping other laser parameters constant, directly modulates the pulse overlap and the number of pulses delivered per unit area. This, in turn, dictates the final surface characteristics. The calculated overlapping parameters for each scanning velocity, derived from Eqs. (1)-(3), are summarized in Table 3.

Table 3. Pulse overlapping parameters of the irradiated samples with different scanning velocities.

v (μm/s)	N	b(μm)	S_{pulse}(%)
60	33.3	6	97
200	11	20	90
300	7.3	30	86
400	5.5	40	81

As summarized in Table 3, increasing the scanning velocity leads to a progressive reduction in both the effective number of overlapping pulses and the spatial pulse overlap percentage. These parameters fundamentally dictate the cumulative thermal accumulation, thereby governing the resulting surface morphology and chemical evolution (Fig. 1 and Table 1). The findings reveal a distinct processing threshold around 200 μm/s, demarcating a transition in surface functionality.

Identifying this operational threshold is essential for optimizing laser processing in industrial workflows, where translation speed directly impacts throughput and manufacturing costs. Specifically, the wettability measurements (Table 2) demonstrate that scanning speeds between 200 and 400 μm/s consistently achieve full superhydrophilicity (WCA≈0∘). This indicates that a velocity of 200 μm/s is already sufficient to reach the target wetting state, offering more than a three-fold increase in throughput compared to the 60 μm/s condition without compromising wetting performance. Moreover, the highest antibacterial efficacy (i.e., minimal bacterial adhesion) was attained at 400 μm/s. Consequently, spatial pulse overlap serves as a tunable design parameter, enabling a strategic trade-off between maximizing processing throughput (200 μm/s) and achieving peak antibacterial performance (400 μm/s).

IV. CONCLUSION

In this study, nanosecond Nd:YAG laser surface texturing was successfully employed to tailor the surface morphology, chemical composition, wettability, and antibacterial properties of 304 stainless-steel by modulating the laser pulse overlap through beam scanning velocity. Field Emission Scanning Electron Microscopy (FESEM) and Energy-dispersive X-ray spectroscopy (EDS) analyses confirmed the formation of dense micro/nanoscale hierarchical structures and a substantial (~13-fold) increase in surface oxidation under ambient processing conditions. Wettability measurements revealed a transition to a superhydrophilic regime at higher scanning velocities (200–400 μm/s), driven by the

[Downloaded from mail.ijop.ir on 2026-11-23]

synergistic effects of laser-induced oxidation and amplified surface roughness.

Biological assays against Escherichia coli demonstrated that bacterial anti-adhesion and bactericidal performance are strongly dictated by the degree of pulse overlap. The surface treated at a scanning velocity of 400 μm/s (corresponding to an 81% pulse overlap) achieved the optimal bactericidal efficacy, reducing bacterial adhesion by 62%. Importantly, this optimized higher scanning velocity concurrently minimizes adverse thermal accumulation and significantly reduces industrial processing time and operational costs. These findings highlight the precise control of pulse overlap as an effective, scalable, and single-step strategy for fabricating functional, antibacterial stainless-steel surfaces for biomedical and industrial applications. Future work will investigate laser treatments across varied fluences and evaluate the long-term durability of these antibacterial properties under physiological flow conditions.

REFERENCES

[1] M. Bencina, T. Mavric, I. Junkar, A. Bajt, A. Krajnovic, K. Lakota, P. Zigon, S. Sodin-Semrl, V. Kralj-Iglic, and A. Iglic, "The importance of antibacterial surfaces in biomedical applications," in Advances in Biomembranes and Lipid Self-Assembly, Vol. 28, A. Iglic, P. Losada Perez, and M. Rappolt, Eds. Elsevier, pp. 115–165, 2018.

[2] R. Kaur and S. Liu, "Antibacterial surface design – Contact kill," Prog. Surf. Sci., Vol. 91, pp. 136–153, 2016.

[3] F.M. Zuki, R.G.J. Edyvean, H. Pourzolfaghar, and N. Kasim, "Modeling of the van der Waals forces during the adhesion of capsule-shaped bacteria to flat surfaces," Biomimetics, Vol. 6, pp. 5(2–16), 2021.

[4] A. Terada, A. Yuasa, T. Kushimoto, S. Tsuneda, A. Katakai, and M. Tamada, "Bacterial adhesion to and viability on positively charged polymer surfaces," Microbiology, Vol. 152, pp. 3575–3583, 2006.

[5] M. Fletcher and J. H. Pringle, "The effect of surface free energy and medium surface tension on bacterial attachment to solid surfaces," J. Colloid Interface Sci., Vol. 104, pp. 5–14, 1985.

[6] D.L. Sanders, A.N. Kingsnorth, J. Lambie, P. Bond, R. Moate, and J.A. Steer, "An experimental study exploring the relationship between the size of bacterial inoculum and bacterial adherence to prosthetic mesh," Surg. Endosc., Vol. 27, pp. 978–985, 2013.

[7] K. Yang, J. Shi, L. Wang, Y. Chen, C. Liang, L. Yang, and L.-N. Wang, "Bacterial anti-adhesion surface design: Surface patterning, roughness and wettability: A review," J. Mater. Sci. Technol., Vol. 99, pp. 82–100, 2022.

[8] A. Francone, S. Merino, A. Retolaza, J. Ramiro, S.A. Alves, J.V. de Castro, N.M. Neves, A. Arana, J.M. Marimon, C.M. Sotomayor Torres, and N. Kehagias, "Impact of surface topography on the bacterial attachment to micro- and nano-patterned polymer films," Surf. Interfaces, Vol. 27, pp. 101494(1–11), 2021.

[9] Q. Pan, Y. Cao, W. Xue, D. Zhu, W. Liu, "Picosecond laser-textured stainless steel superhydrophobic surface with an antibacterial adhesion property," Langmuir, Vol. 35, pp. 11414–11421, 2019.

[10] X. Zhang, L. Wang, and E. Levanen, "Superhydrophobic surfaces for the reduction of bacterial adhesion," Royal Soc. Chem. (RSC) Adv., Vol. 3, pp. 12003–12020, 2013.

[11] S. Sohrabi, H. Pazokian, B. Ghafary, and M. Mollabashi, "Super-hydrophilic nano-structured surface with antibacterial properties," Opt. Mater. Express, Vol. 14, pp. 116–124, 2024.

[12] S. Shin, J. Seo, H. Han, S. Kang, H. Kim, and T. Lee, "Bio-inspired extreme wetting surfaces for biomedical applications," Mater., Vol. 9, pp. 116(1–26), 2016.

[13] M.V. Shugaev, M. He, Y. Levy, A. Mazzi, A. Miotello, N.M. Bulgakova, and L.V. Zhigilei, "Laser-induced thermal processes: heat transfer, generation of stresses, melting and solidification, vaporization, and phase explosion," in Handbook of Laser Micro- and Nano-Engineering, K. Sugioka, Ed. Cham: Springer, pp. 83–163, 2021.

[14] M. Iqbal, D.K. Dinh, Q. Abbas, M. Imran, H. Sattar, and A.U. Ahmad, "Controlled surface wettability by plasma polymer surface

[Downloaded from mail.ijop.ir on 2026-11-23]

modification," Surfaces, Vol. 2, pp. 349–371, 2019.

[15] A. Cunha, A.-M. Elie, L. Plawinski, A.P. Serro, A.M.B. do Rego, A. Almeida, M.C. Urdaci, M.-C. Durrieu, and R. Vilar, "Femtosecond laser surface texturing of titanium as a method to reduce the adhesion of Staphylococcus aureus and biofilm formation," Appl. Surf. Sci., Vol. 360, pp. 485–493, 2016.

[16] N. Epperlein, F. Menzel, K. Schwibbert, R. Koter, J. Bonse, J. Sameith, J. Kruger, and J. Toepel, "Influence of femtosecond laser produced nanostructures on biofilm growth on steel," Appl. Surf. Sci., Vol. 418, pp. 420–424, 2017.

[17] R.K. Gupta, B. Anandkumar, A.K. Choubey, R. P. George, P.S. Ganesh, B.N. Upadhyaya, J. Philip, K.S. Bindra, and R. Kaul, "Antibacterial and corrosion studies on nanosecond pulse laser textured 304 L stainless steel surfaces," Lasers Manuf. Mater. Process., Vol. 6, pp. 332-343, 2019.

[18] R. Gupta, A. Gaddam, H. Naveena, D. Prajapati, S. Dimov, D. Bhatia, A. Mishra, Y. Sofronov, and M. Vadali, "Improving the cell adhesion and antibacterial behaviour on Ti6Al4V through micro and nano hierarchical laser surface texturing," Surf. Interfaces, Vol. 58, pp. 105857(1–13), 2025.

[19] H. Pazokian, "Theoretical and experimental investigations of the influence of overlap between the laser beam tracks on channel profile and morphology in pulsed laser machining of polymers," Optik, Vol. 171, pp. 431–436, 2018.

[20] N. Kumar, S. Prakash, and S. Kumar, "Studies of laser textured Ti-6Al-4V wettability for implants," IOP Conf. Ser.: Mater. Sci. Eng., Vol. 149, pp. 012056(1–5), 2016.

[21] S. Sohrabi, H. Pazokian, B. Ghafary, M. Mollabashi, and M. Montazerolghaem, "Improving the antibacterial performance of 304 stainless steel using Nd-YAG laser irradiation," Appl. Phys. A, Vol. 130, pp. 104(1–6), 2024.

[22] B. Jin and X. Xu, "Machine learning predictions of regional steel price indices for east China," Ironmak. Steelmak., Vol. 52, pp. 368–381, 2025.

[23] B. Jin and X. Xu, "Contemporaneous causality among price indices of ten major steel products," Ironmak. Steelmak., Vol. 51, pp. 515–526, 2024.

[24] B. Jin and X. Xu, "Predicting open interest in thermal coal futures using machine learning," Miner. Econ., Vol. 38, pp. 795–809, 2025.

[25] B. Jin, X. Xu, "Forecasts of coking coal futures price indices through Gaussian process regressions," Miner. Econ., Vol. 38, pp. 203-217, 2025.

[26] Y. Zhang and X. Xu, "Machine learning surface roughnesses in turning processes of brass metals," Int. J. Adv. Manuf. Technol., Vol. 121, pp. 2437–2444, 2022.

[27] Y. Zhang, X. Xu, "Machine learning cutting force, surface roughness, and tool life in high-speed turning processes," Manuf. Lett., Vol. 29, pp. 84–89, 2021.

[28] Y. Zhang and X. Xu, "Machine learning modeling of metal surface energy," Mater. Chem. Phys., Vol. 267, pp. 124622(1–6), 2021.

[29] F.R. Marciano, D.A. Lima-Oliveira, N.S. Da-Silva, A.V. Diniz, E.J. Corat, and V.J. Trava-Airoldi, "Antibacterial activity of DLC films containing TiO_2 nanoparticles," J. Colloid Interface Sci., Vol. 340, pp. 87–92, 2009.

[30] L. Li, L. Yang, Y. Liao, H. Yu, Z. Liang, B. Zhang, X. Lan, R. Luo, and Y. Wang, "Superhydrophilic versus normal polydopamine coating: A superior and robust platform for synergistic antibacterial and antithrombotic properties," Chem. Eng. J., Vol. 402, pp. 126196(1–10), 2020.

[31] J. Xu, Y. Zhao, Y. Chen, Y. Chen, Z.-H. Xie, and P.R. Munroe, "A superhydrophilic, light/microwave-absorbing coating with remarkable antibacterial efficacy," Am. Chem. Soc. (ACS) Appl. Mater. Interfaces, Vol. 14, pp. 42468–42482, 2022.

[32] P. Henke, H. Kozak, A. Artemenko, P. Kubat, J. Forstova, and J. Mosinger, "Superhydrophilic polystyrene nanofiber materials generating $O_2(^1\Delta g)$: Postprocessing surface modifications toward efficient antibacterial effect," Am. Chem. Soc. (ACS) Appl. Mater. Interfaces, Vol. 6, pp. 13007-13014, 2014.

[33] X. Wu, X. Zou, D. Wang, M. Li, B. Zhao, Y. Xia, H. Wang, and C. Liang, "Revealing the mechanical impact of biomimetic nanostructures on bacterial behavior," Coatings, Vol. 14, pp. 860(1–18), 2024.

[Downloaded from mail.ijop.ir on 2026-11-23]

[34] M. Ozdal and S. Gurkok, "Recent advances in nanoparticles as antibacterial agent," Abs., Distrib., Metabol., Excret., and Toxicity (ADMET) Drug Metabol. Pharmacokinetics (DMPK), Vol. 10, pp. 115–129, 2022.



Hedieh Pazokian was born in Tehran, Iran. She received her BSc degree in physics from Semnan University in 2004. She obtained MSc and PhD degrees in physics from Iran University of Science and Technology in 2006 and 2011, respectively.

Her current research interest includes laser-material interaction, laser induced graphene, optical materials fabrication, optofluidic, laser nanotechnology and nano photonics.



Sahar Sohrabi was born in Semnan, Iran. She received her BSc, MSc, and PhD degrees in atomic and molecular physics from Iran University of Science and Technology in 2015, 2017, and 2024, respectively.

Now, she is a post-doctoral researcher in Quantum Key Distribution (QKD).

Her current research interests include laser-material interaction, laser induced surface phenomena and quantum cryptography.

[Downloaded from mail.ijop.ir on 2026-11-23]

THIS PAGE IS INTENTIONALLY LEFT BLANK.

[Downloaded from mail.ijop.ir on 2026-11-23]